SCIENCE CHINA
Technological Sciences

• Article •

doi: 10.1007/s11431-016-0355-3

Prediction of stall inception in multi-stage compressors based on an eigenvalue approach

CHENG FanJie, SUN DaKun*, DONG Xu & SUN XiaoFeng

School of Energy and Power Engineering, Beihang University, Beijing 100191, China

Received May 3, 2016; accepted January 1, 2017; published online April 20, 2017

A stability model for multi-stage compressor is developed on the basis of the eigenvalue approach. This model assumes that the unsteady flow field can be decomposed into pressure, vortex and entropy waves. Besides, a linear cascade of blades is modeled by three-dimensional semi-actuator disk theory and the characteristics of steady flow field are also considered in the present model. The connection between the analytical solution for stator, rotor and gap can be established by applying mode matching approach, the relevant stability equation can be expressed in the form of matrix, while the compressor system stability can be judged by the imaginary part of the matrix eigenvalue. The capacity of the stall inception model to predict the stall inception point of multi-stage compressor is assessed against the experimental data of National Aeronautics and Space Administration (NASA) two stage fan. The theoretical results show that this model can predict the stall onset points of a two-stage fan at different operating speeds with a reasonable accuracy.

multi-stage compressor, unsteady flow, rotating stall, stability model, stall inception

Citation: Cheng F J, Sun D K, Dong X, et al. Prediction of stall inception in multi-stage compressors based on an eigenvalue approach. Sci China Tech Sci, 2017, 60: doi: 10.1007/s11431-016-0355-3

1 Introduction

The flow instabilities have already seriously restricted the further development of multi-stage compressors. It is often noted that the stable operating range of a well-designed compressor with high total-pressure ratio and high efficiency often cannot meet the expected requirement of stall margin. The researchers have done considerable work to understand and avoid these problems and many progresses have been achieved, however, there are still many problems that have to be surmounted. One of the most important problems is how to predict the stability of a multi-stage compressor, especially in the design stage.

Generally, there are two kinds of methods to investigate the stall inception of compressors: numerical computation method, semi-analytical and semi-numerical method.

The numerical computation method can consider more details of geometric and aerodynamic parameters by solving Euler or Navier-Stokers equations. Hendricks et al. [1] developed a nonlinear, two-dimensional, compressible model to study rotating stall/surge inception and evolution on a high speed, multi-stage compressor. Their simulations of the rotating stall evolution before surge were in agreement with the experimental results. In a similar investigation, Longley et al. [2] have done a calculation work about how the flow field breakdown of a four-stage compressor is affected by inlet distortions at different operating speeds. He [3] conducted a computational study of rotating stall inception in axial compressors by using a numerical model with a quasi-three-dimensional time marching Navier-Stokes solver. It should be noted that the pattern of rotating stall inception is sensitive to external disturbances in a form of a rotational or station-

*Corresponding author (email: sundk@buaa.edu.cn)

ary circumferential non-uniformity. Gong et al. [4] developed a three dimensional nonlinear computational model for simulating the stall inception of a multi-stage compressor. In this model, each blade row was represented by a kind of body force that is formulated in terms of the blade's pressure rise and flow turning characteristics. There is another type of model [5–8] with the application of the perturbation form of body force, which can also include the effects of complex geometric parameters (blade shapes, blade tip clearances and so on) on stall inception in axial/centrifugal compressors. In this type of model, the compressor stability can be descripted as an eigenvalue problem and the singular value decomposition (SVD) method is adopted to solve the large scale complex eigenvalue problems. The advantages of this eigenvalue method over the existing approach as initial boundary value problem is much less time cost. In fact, Chen et al. [9] conducted a series of single stage compressor simulations with full-annulus grid to model the 3D, viscous, unsteady blade row interaction without artificial inlet distortion. And ideally, the simulation time for each speedline usually was 0.5×10^6 CPU hours.

Although the numerical computation method can consider more aerodynamic and geometric characteristics of single stage compressor, it is still especially difficult to make the stability prediction of multi-stage compressor. However, the 2D models could not capture the stall inception with a satisfactory accuracy, while the 3D simulations are also dependent on the setup of the boundary conditions, the approaches of the numerical scheme and the types of initial disturbances and so on. In addition, the cost of computational resources are too high to be used in engineering fields with both the 3D unsteady simulations and the eigenvalue method with the body force, even for single stage compressor.

On the other hand, the semi-analytical and semi-numerical method describes the rotating stall as eigenvalue models based on the small disturbance theory. The early investigations focused on the prediction of propagation speed and number of stall cells. The pioneering works have been reported by Sears [10], Emmons et al. [11]. As Day [12] mentioned in his review paper, the small disturbance theories were not really successful in predicting stall cell speed and numbers. The reason has been stated by Stenning [13] in 1980, the fully developed rotating stall is a highly developed nonlinear phenomenon. In fact, the true purpose of the linearized small disturbance theories is precisely predicting the stall inception before the fully developed rotating stall. The research history has shown that there were many attentions paid on the prediction of inception conditions. Nenni and Ludwig [14] established a 2D incompressible model to deal with the stall inception in a two blade rows and a single blade row. The prediction results indicated that the blade row loss and flow turning characteristics were very important to a linearized stability theory. Later, Ludwig and Nenni [15] further developed a 3D incompressible model, but there were no reasonable numerical examples to demonstrate the model's effectiveness and reliability in the public literature. Bonnaure [16] developed a 2D compressible stability model with the effects of the vortical mode and the entropy mode. Takata and Nagashima [17] presented a work about the rotating stall in three-dimensional blade rows subjected to a spanwise sheared inlet flow. Gordon [18] reported two types of 3D incompressible stability models with radial flow variations by using an actuator-disk model and a distributed body force model, respectively.

2D models are restricted by the lack of flow variations along the spanwise direction. Due to the shrunk flow path is induced by the compressible characteristics in high speed compressor, the spanwise variation of the aerodynamic parameters is too obvious to be ignored, especially with the development of the modern highly loaded compressor. In addition, Gorrell et al. [19] found that the change of radial profile of pressure ratio caused by casing treatments could have an important impact on compressor stability, and the investigations also demonstrated the effect of the radial flow variations on stall inception. In order to enlarge the valid application range of the compressor stability model, it is essential to include the three-dimensional effects into the 3D compressible stall inception model.

In recent years, more attention has been paid on the inception condition of rotating stall, and a 3D compressible stability model [20–22] was established to consider the spanwise variation effects, and then this model can also consider the effects of shock wave and complicated boundary condition on stall inception. The results show that this approach is effective on the stall inception prediction and the novel casing treatment design in subsonic/transonic compressors [23–27]. Although a lot of theoretical work has been conducted to predict the stall inception condition, up to now the predictions of stall inception by using the 3D compressible stability model are only conducted in single stage compressors.

In the present study, a 3D multi-stage compressor stability model is established. On the basis of the stall inception model, the prediction of the stall onset point of a multi-stage compressor is carried out. And the comparison with National Aeronautics and Space Administration (NASA) two stage fan's experiment [28] validates the effectiveness and accuracy of this model.

2 Theretical model of stall inception for multi-stage compressor

2.1 Governing equation

The flow can be assumed to be small amplitude perturbation for more attention is put on the inception condition of rotating stall. Based on the small disturbance theory, small perturba-

tions are added to each of the variables in the equations.

Depending on the response to the unsteady small amplitude flow disturbance in the form of $x = Ae^{i\omega t}$, the dynamic system stability can be judged by the imaginary part of the eigenvalue ω_i. If ω_i is positive, the small disturbance will decrease and the system is stable. In contrast, the small disturbance will grow up and the system is unstable. It should be noted that the real part of the eigenvalue ω_r is related to the propagation speed of stall inception.

In the present model, the 3D compressible linearized Euler equations are adopted as the governing equations for the stall inception prediction, and the linearized form of the equations are shown as follows

$$\frac{\partial \rho}{\partial t} + \nabla \cdot (\rho \boldsymbol{V}) = 0, \tag{1}$$

$$\frac{\mathrm{D}\boldsymbol{V}}{\mathrm{D}t} + \frac{1}{\rho_0}\nabla p = 0, \tag{2}$$

$$\frac{1}{P_0}\frac{\mathrm{D}p}{\mathrm{D}t} - \frac{k}{\rho_0}\frac{\mathrm{D}\rho}{\mathrm{D}t} = 0, \tag{3}$$

where $\boldsymbol{V}$ is the velocity, P_0 is the mean pressure, ρ_0 is the mean density, p is the disturbance pressure, ρ is the disturbance density, t means time, and k is the specific heat ratio.

2.2 Analytical solutions of basic equations

For a multi-stage compressor, its general structure can be illustrated as Figure 1. The X^j is a reference plane at the leading edge of arbitrary blade row k with the chord length c and the stagger angle θ. The L^{j+1} is the distance between plane X^{j+1} and the trailing edge of the row k.

A stability model can be established based on an eigenvalue theory as shown in Figure 2. First, analytical solutions in bladed/unbladed region are derived, respectively. It should be noted that the solution consists of pressure wave propagating upstream or downstream, vortex wave and entropy wave convecting with the mean flow. Then matching conditions at the interface between blade/unbladed region and the inlet/outlet boundary conditions are adopted to reflect the loss characteristics and flow deflection of the compressor. Finally, a group of homogeneous equations can be yield and the stability equation will be established.

Figure 1 also shows the Schematic of a two-stage compressor unwrapped in circumferential direction. The blade height is h and the x, y, z are axial, circumferential and radial coordinates, respectively. In this model, the uniform flow can be descripted to be compressible, inviscid, and non-heat-conductive. For solid wall case, the casing and hub are rigid. The wave lengths of flow disturbances are assumed to be much larger than blade spacing s in the circumferential direction.

2.2.1 *Analytical solutions of basic equations in an unbladed region*

In an unbladed region, the 3D compressible linearized Euler equations (1)–(3) can be solved by the separation variable method and series expansion approach. Considering the effect of vortex wave and entropy wave, the analytical solutions are expressed as follows.

Fluctuating pressure:

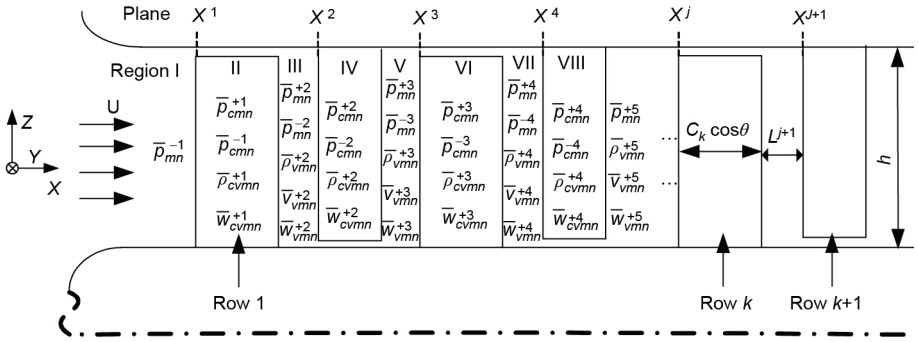

Figure 1 Schematic of a multi-stage compressor.

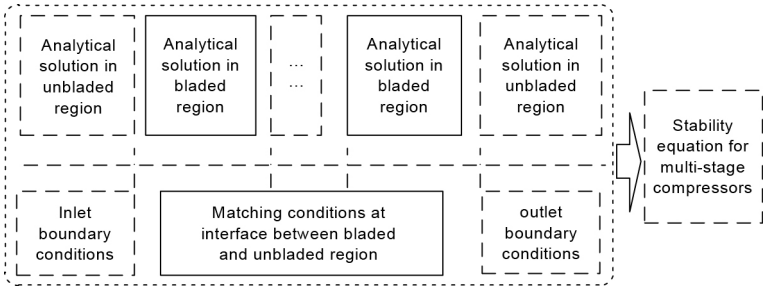

Figure 2 General structural schematic of the multi-stage compressor stability model.

$$p^j(x,y,z,t) = \sum_{m=-\infty}^{+\infty}\sum_{n=1}^{+\infty}\left[\overline{p}_{mn}^{+j} e^{i\alpha_{mn}^{+j}(x-x^j)}\psi_{mn}^{+j}(z) + \overline{p}_{mn}^{-j} e^{i\alpha_{mn}^{-j}(x-x^j)}\psi_{mn}^{-j}(z)\right] e^{i\left(\beta_m y+\omega t\right)}; \tag{4}$$

Fluctuating density:

$$\rho^j = \sum_{m=-\infty}^{+\infty}\sum_{n=1}^{+\infty}\left[\frac{1}{\left(a_0^j\right)^2}\left(\psi_{mn}^{+j}(z)e^{i\alpha_{mn}^{+j}(x-x^j)}\overline{p}_{mn}^{+j} + \psi_{mn}^{-j}(z)e^{i\alpha_{mn}^{-j}(x-x^j)}\overline{p}_{mn}^{-j}\right) + \overline{\rho}_{vmn}^{+j}\psi_{vmn}^{+j}(z)e^{-i\frac{\omega+\beta_m V}{U}(x-x^j)}\right] e^{i\left(\beta_m y+\omega t\right)}; \tag{5}$$

Fluctuating velocity:

$$u^j = \sum_{m=-\infty}^{+\infty}\sum_{n=1}^{+\infty}\left[-\frac{1}{\rho_0^j}\left(\frac{\alpha_{mn}^{+j}\psi_{mn}^{+j}(z)e^{i\alpha_{mn}^{+j}(x-x^j)}\overline{p}_{mn}^{+j}}{\left(\omega+\alpha_{mn}^{+j}U^j+\beta_m V^j\right)} + \frac{\alpha_{mn}^{-j}\psi_{mn}^{-j}(z)e^{i\alpha_{mn}^{-j}(x-x^j)}\overline{p}_{mn}^{-j}}{\left(\omega+\alpha_{mn}^{-j}U^j+\beta_m V^j\right)}\right) + \left(\frac{\beta_m U\overline{v}_{vmn}^{+j}}{\omega+\beta_m V} - \frac{ik_{vmn}^{+j}U\overline{w}_{vmn}^{+j}}{\omega+\beta_m V}\right)\psi_{vmn}^{+j}(z)e^{-i\frac{\omega+\beta_m V}{U}(x-x^j)}\right] e^{i\left(\beta_m y+\omega t\right)}, \tag{6}$$

$$v^j = \sum_{m=-\infty}^{+\infty}\sum_{n=1}^{+\infty}\left[-\frac{1}{\rho_0^j}\left(\frac{\beta_m\psi_{mn}^{+j}(z)e^{i\alpha_{mn}^{+j}(x-x^j)}\overline{p}_{mn}^{+j}}{\left(\omega+\alpha_{mn}^{+j}U^j+\beta_m V^j\right)} + \frac{\beta_m\psi_{mn}^{-j}(z)e^{i\alpha_{mn}^{-j}(x-x^j)}\overline{p}_{mn}^{-j}}{\left(\omega+\alpha_{mn}^{-j}U^j+\beta_m V^j\right)}\right) + \overline{v}_{vmn}^{+j}\psi_{vmn}^{+j}(z)e^{-i\frac{\omega+\beta_m V}{U}(x-x^j)}\right] e^{i\left(\beta_m y+\omega t\right)}, \tag{7}$$

$$w^j = \sum_{m=-\infty}^{+\infty}\sum_{n=1}^{+\infty}\left[\frac{1}{\rho_0^j}\left(\frac{k_{mn}^{+j}\phi_{mn}^{+j}(z)e^{i\alpha_{mn}^{+j}(x-x^j)}\overline{p}_{mn}^{+j}}{i\left(\omega+\alpha_{mn}^{+j}U^j+\beta_m V^j\right)} + \frac{k_{mn}^{-j}\phi_{mn}^{-j}(z)e^{i\alpha_{mn}^{-j}(x-x^j)}\overline{p}_{mn}^{-j}}{i\left(\omega+\alpha_{mn}^{-j}U^j+\beta_m V^j\right)}\right) + \overline{w}_{vmn}^{+j}\phi_{vmn}^{+j}(z)e^{-i\frac{\omega+\beta_m V}{U}(x-x^j)}\right] e^{i\left(\beta_m y+\omega t\right)}, \tag{8}$$

where m and n are circumferential and radial mode number, x^j is axial coordinates for the plane X^j. It is noted that ω is the eigen-frequency of the dynamic system, and its imaginary part indicates the stability of the compressor system.

The axial wave numbers $\alpha_{mn}^{\pm j}$ are

$$\alpha_{mn}^{\pm j} = \frac{M_x\left(\beta_m M_y + \frac{\omega}{a_0}\right) \pm \sqrt{\Lambda}}{\left(1-M_x^2\right)}, \tag{9}$$

where $\Lambda = \left(\beta_m M_y + \frac{\omega}{a_0}\right)^2 + \left(1-M_x^2\right)\left[\beta_m^2 + \left(k_{mn}^{\pm j}\right)^2\right]$, in which the radial wave number is $k_{mn} = n\pi/h$ $(n = 0,1,2,...,N)$, $\beta_m = m/r_m$, r_m is the mean radius, M_x and M_y are axial and circumferential Mach numbers, a_0 is the sound speed, "$+j$" and "$-j$" represent the waves traveling downstream and upstream from the plane X^j, respectively.

The rigid wall boundary condition will result in the radial eigenfunctions in the form

$$\psi_{mn}^{\pm j}(z) = \psi_{vmn}^{\pm j}(z) = \cos\left(k_{vmn}^{\pm j}z\right), \tag{10}$$

$$\phi_{mn}^{\pm j}(z) = \phi_{vmn}^{\pm j}(z) = \sin\left(k_{vmn}^{\pm j}z\right). \tag{11}$$

In order to determine the small disturbances with a corresponding mode wave (m, n), there are 5 mode coefficients that need to be provided in an unbladed region: $\overline{p}_{mn}^{+j}, \overline{p}_{mn}^{-j}, \overline{v}_{vmn}^{+j}, \overline{w}_{vmn}^{+j}, \overline{\rho}_{vmn}^{+j}$, where $\overline{p}_{mn}^{+j}$ and $\overline{p}_{mn}^{-j}$ represent the wave amplitude corresponding to acoustic mode related to pressure variation, $\overline{v}_{vmn}^{+j}$ and $\overline{w}_{vmn}^{+j}$ are the vortical mode, and $\overline{\rho}_{vmn}^{+j}$ is related to the entropy mode.

2.2.2 *Analytical solutions of basic equations in a bladed region*

In the present study, a linear cascade of blades is modeled as a 3D semi-actuator disk composed of flat-plate airfoils with chord length c, spacing s and stagger angle θ as shown in Figure 3.

In the blade channel, the mean flow is assumed to turn along the blade chord direction at the leading edge and to be one-dimensional channel flow. The fluctuating velocity has radial and chord-wise components without circumferential component in the cascade. The transformation and rotation of the coordinates system are illustrated as Figure 4. Where Ω is the rotating frequency and Ω=0 means that the blade cascade is a stator.

The analytical solutions in bladed region can also be obtained like those solutions in unbladed regions.

Fluctuating pressure:

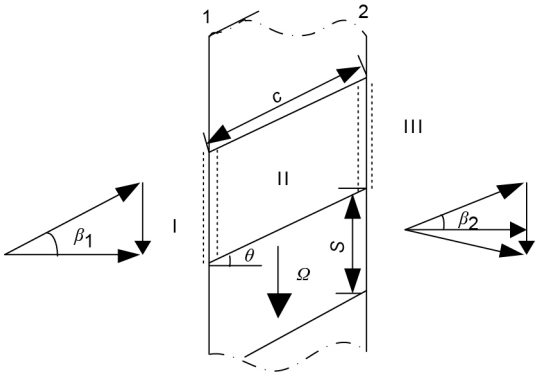

Figure 3 Schematic of a linear cascade blades described by semi-actuator disk.

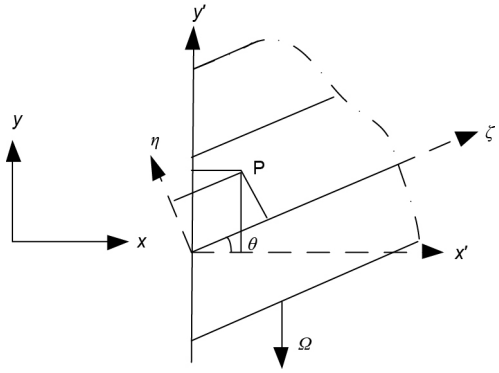

Figure 4 Transformation of coordinates system in bladed region.

$$p_c^k(x,y',z,t)=\sum_{m=-\infty}^{+\infty}\sum_{n=1}^{+\infty}\left[e^{i\alpha_{cmn}^{+k}(x-x^k)}\psi_{cmn}^{+k}(z)\overline{p}_{cmn}^{+k}+e^{i\alpha_{cmn}^{-k}(x-x^k)}\psi_{cmn}^{-k}(z)\overline{p}_{cmn}^{-k}\right]e^{i(\omega-m\Omega)t+i\beta_m y'}; \tag{12}$$

Fluctuating density:

$$\rho_c^k(x,y',z,t)=\sum_{m=-\infty}^{+\infty}\sum_{n=1}^{+\infty}\left[\begin{array}{l}\dfrac{1}{\left(a_0^k\right)^2}\left(\psi_{cmn}^{+k}(z)e^{i\alpha_{cmn}^{+k}(x-x^k)}\overline{p}_{cmn}^{+k}+\psi_{cmn}^{-k}(z)e^{i\alpha_{cmn}^{-k}(x-x^k)}\overline{p}_{cmn}^{-k}\right)+\\ \overline{\rho}_{cvmn}^{+k}\psi_{cvmn}^{+k}(z)e^{-i\frac{(\omega-m\Omega)+\beta_m W_c^k\sin\theta^k}{W_c^k\cos\theta^k}(x-x^k)}\end{array}\right]e^{i(\omega-m\Omega)t+i\beta_m y'}; \tag{13}$$

Fluctuating chord-wise velocity:

$$q_c^k(x,y',z,t)=\sum_{m=-\infty}^{+\infty}\sum_{n=1}^{+\infty}\left[\begin{array}{l}-\dfrac{1}{\rho_0^k}\left(\begin{array}{l}\dfrac{\left(\alpha_{cmn}^{+k}\cos\theta+\beta_m\sin\theta\right)e^{i\alpha_{cmn}^{+k}(x-x^k)}\psi_{cmn}^{+k}(z)\overline{p}_{cmn}^{+k}}{\left[(\omega-m\Omega)+W_c\left(\alpha_{cmn}^{+k}\cos\theta+\beta_m\sin\theta\right)\right]}+\\ \dfrac{\left(\alpha_{cmn}^{-k}\cos\theta+\beta_m\sin\theta\right)e^{i\alpha_{cmn}^{-k}(x-x^k)}\psi_{cmn}^{-k}(z)\overline{p}_{cmn}^{-k}}{\left[(\omega-m\Omega)+W_c\left(\alpha_{cmn}^{-k}\cos\theta+\beta_m\sin\theta\right)\right]}\end{array}\right)\\ -\dfrac{ik_{cvmn}^{+k}W_c^k}{(\omega-m\Omega)}e^{-i\frac{(\omega-m\Omega)+\beta_m W_c^k\sin\theta^k}{W_c^k\cos\theta^k}(x-x^k)}\psi_{cvmn}^{+k}(z)\overline{w}_{cvmn}^{+k}\end{array}\right]e^{i(\omega-m\Omega)t+i\beta_m y'}; \tag{14}$$

Fluctuating radial velocity:

$$w_c^k(x,y',z,t)=\sum_{m=-\infty}^{+\infty}\sum_{n=1}^{+\infty}\left[\begin{array}{l}\dfrac{1}{\rho_0}\left(\begin{array}{l}\dfrac{k_{cmn}^{+k}e^{-i\alpha_{cmn}^{+k}(x-x^k)}\phi_{cmn}^{+k}(z)\overline{p}_{cmn}^{+k}}{i\left[(\omega-m\Omega)+W_c\left(\alpha_{cmn}^{+k}\cos\theta+\beta_m\sin\theta\right)\right]}+\\ \dfrac{k_{cmn}^{+k}e^{-i\alpha_{cmn}^{-k}(x-x^k)}\phi_{cmn}^{-k}(z)\overline{p}_{cmn}^{-k}}{i\left[(\omega-m\Omega)+W_c\left(\alpha_{cmn}^{-k}\cos\theta+\beta_m\sin\theta\right)\right]}\end{array}\right)\\ +\overline{w}_{cvmn}^{+k}\phi_{cvmn}^{+k}(z)e^{-i\frac{(\omega-m\Omega)+\beta_m W_c^k\sin\theta^k}{W_c^k\cos\theta^k}(x-x^k)}\end{array}\right]e^{i(\omega-m\Omega)t+i\beta_m y'}, \tag{15}$$

where W_c represents the relative inflow velocity, q and w are the chord-wise and radial fluctuating velocities, subscript c means the relative parameters in the cascade. There are 4 mode coefficients that need to be provided in a bladed region: $\overline{p}_{cmn}^{+k}$, $\overline{p}_{cmn}^{-k}$, $\overline{w}_{cvmn}^{+k}$, $\overline{p}_{cvmn}^{+k}$.

As shown in Figure 1, for a two-stage compressor with rigid

wall configuration, the flow field can be divided into 9 regions by 8 interface planes, and there are 36 mode coefficients in the bladed and unbladed regions, respectively.

2.3 Matching conditions

After obtaining the analytical solutions of basic equations, the relationships between these small disturbances at the interface planes can be established by matching conditions and the eigenvalue equations for the compressor stability can also be yielded.

As we know, the total pressure loss and flow turning characteristics are very important to the prediction results. In this model, the flow turning and loss are assumed to occur at the blade leading edge and the matching conditions can be given as below.

Mass conservation:

$$\rho^j U^j + \rho_0^j u^j = \left(\rho^k U^k + \rho_0^k q^k\right)\cos\theta^k; \tag{16}$$

Relative total temperature conservation:

$$\begin{aligned} T'^j_t &= \frac{p^j}{R\rho_0} - \frac{\left(a_0^j\right)^2}{kR\rho_0}\rho^j + \frac{1}{c_p}\left(U^j u^j + V_r^j v^j\right) \\ &= \frac{p^k}{R\rho_0} - \frac{\left(a_0^k\right)^2}{kR\rho_0}\rho^k + \frac{W_c^k q^k}{c_p} = T'^k_t; \end{aligned} \tag{17}$$

Continuity of radial velocity:

$$w^k = w^{j+1}; \tag{18}$$

Relative total pressure relation:

$$\begin{aligned} p_t^j - p_t^k = \frac{1}{1+i\omega\tau_{\text{loss}}}\Bigg[&\frac{1}{2}\xi_s^k\rho^j\left(W^j\right)^2 + \xi_s^k\rho_0^j\left[U^j u^j + V_r^j v^j\right] \\ &+ \frac{1}{2U^j}\frac{\partial\xi_s^k}{\partial\tan\beta^k}\rho_0^j\left(W^j\right)^2\left(v^j - u^j\tan\beta^k\right)\Bigg], \end{aligned} \tag{19}$$

where τ_{loss} is time delay, and ξ_s^k is relative total-pressure loss coefficient: $\xi_s^k = \dfrac{P_t^j - P_t^{j+1}}{\rho^j\left(W^j\right)^2/2}$.

Fluctuating total pressure in an unbladed region:

$$\begin{aligned} p_t^j = &\left(S_1^j - \frac{k\left(M^j\right)^2}{2}S_2^j\right)p^j + \frac{\left(W^j\right)^2}{2}S_2^j\rho^j \\ &+\rho_0^j U^j S_2^j u^j + \rho_0^j S_2^j V_r^j v^j, \end{aligned} \tag{20}$$

where $S_1^j = \left[1 + \dfrac{\kappa-1}{2}\left(M^j\right)^2\right]^{\frac{\kappa}{\kappa-1}}$, $S_2^j = \left[1 + \dfrac{\kappa-1}{2}\left(M_c^j\right)^2\right]^{\frac{1}{\kappa-1}}$.

Fluctuating total pressure in a bladed region:

$$\begin{aligned} p_t^k = &\left(S_1^k - \frac{k\left(M_c^k\right)^2}{2}S_2^k\right)p^k \\ &+\frac{\left(W_c^k\right)^2}{2}S_2^k\rho^k + \rho_0^k S_2^k W_c^k q^k, \end{aligned} \tag{21}$$

where $S_1^k = \left[1 + \dfrac{\kappa-1}{2}\left(M_c^k\right)^2\right]^{\frac{\kappa}{\kappa-1}}$, $S_2^k = \left[1 + \dfrac{\kappa-1}{2}\left(M_c^k\right)^2\right]^{\frac{1}{\kappa-1}}$.

In this stability model, it is assumed that no flow turning and loss happen at the blade trailing edge, so 5 matching conditions are as follows.

$$p^k = p^{j+1}, \tag{22}$$

$$\rho^k = \rho^{j+1}, \tag{23}$$

$$w^k = w^{j+1}, \tag{24}$$

$$q^k\cos\theta = u^{j+1}, \tag{25}$$

$$q^k\sin\theta = v^{j+1}. \tag{26}$$

Since the small disturbances need to satisfy the periodic condition and there is no energy exchange between each circumferential modes, the phase of the same circumferential mode is coincident. The radial modes also have the coherence phase for a multi-stage compressor with rigid wall.

The phases of the axial modes are $e^{i\alpha^j\left(x-x^j\right)}$ for the solutions in the unbladed region before the row k, $e^{i\alpha^{j+1}\left(x-x^{j+1}\right)}$ for the solutions in the unbladed region after the row k, and $e^{i\alpha^k\left(x-x^k\right)}$ for the solutions in the cascade of the row k, respectively. In matching conditions, the axial phases are all 1 for the all solutions at the blade leading edge, $e^{i\alpha^{j+1}L^{j+1}}$ for the solutions in the unbladed region at the blade trailing edge, and $e^{i\alpha^k c^k\cos\theta^k}$ for the solutions in the bladed region at the blade trailing edge, respectively.

By using the no reflection boundary conditions, the inlet/outlet conditions are yielded $\overline{p}_{mn}^{+1} = \overline{p}_{vmn}^{+1} = \overline{v}_{vmn}^{+1} = \overline{w}_{vmn}^{+1} = \overline{p}_{mn}^{-(J+1)} = 0$ $(n = 0, 1, 2, 3, \cdots, N)$.

2.4 Stability equations of multistage compressors

Based on the mode-matching method, the eigenvalue equation can be derived as

$$Q_{mn}(\omega)_{(9K\times 9K)} \bullet \overline{X}_{mn(9K)} = 0, \tag{27}$$

where K is the number of rows.

Since eq. (27) is a homogeneous equation, a non-trivial solution exists if

$$\det\left[Q_{mn}(\omega)\right] = 0. \tag{28}$$

By solving eq. (28), the compressor stability can be judged by the imaginary part of the eigenvalue ω, while the real part indicates the perturbation frequency. The singular value decomposition (SVD) is adopted to solve the eigenvalue equation. More details about the stability model and the numerical method for solving eigenvalue equation can be found in refs. [5,21,22].

This stall inception prediction model of multi-stage compressor can predict stall inception and assess the stability

trend of compressor according to the characteristics line point by point of different operation speeds. In the experiments with large flow rate, the imaginary part of the eigenvalue is positive, the system is stable. With the decrease of flow rate, the imaginary part of the eigenvalue turns to negative, which means that the operation point is near to the stall point, and we can get the theoretical prediction results.

3 Numerical prediction and comparisons with experimental results

3.1 NASA two-stage fan

In this section, a NASA two-stage fan [28] is chosen to validate the applicability of the compressor stability model on the prediction of stall onset point. The NASA two-stage fan was tested with redesigned low-aspect-ratio first-stage rotor (Figure 5). Detailed experiments were conducted over the entire fan operating flow range at speeds from 50% to 100% design speed. The mass flow was 33.248 kg/s, the total pressure ratio was 2.399 and the adiabatic efficiency was 0.849 at design speed. Table 1 shows some design parameters and Figure 6 shows the overall performance. The two-stage fan is a representative transonic compressor at the design rotation speed, while the spanwise distribution of the inlet relative inlet Mach number range is from 0.55 to 1.05 at 80% design rotation speed. Table 2 shows the relative inlet Mach numbers of the two stage fan at the blade tip. The details of geometrical configuration and performance parameters of this compressor were presented in a NASA report [29] and detailed experimental data were provided by Urasek et al. [28]. And all these data presented here are at 100% and 80% design operating speed, respectively.

3.2 Model validation on NASA two-stage fan at 80% design operating speed

As input data of the stall inception model, the aerodynamic and geometric parameters of the compressor are required. For the NASA two-stage fan, all necessary data can be obtained from the experiment [28].

In this investigation, it should be noted that a kind of extrapolation is adopted to obtain the performance data at the unstable operating point. Take loss coefficient and its derivation to relative inlet angle tangent value, for instance. Firstly, the variation relationship between loss coefficients and flow rates can be fitted by using five experimental data points which are already known, and then the loss coefficients after decrease flow rates can be find out from this relationship. Secondly, the variation relationship between all the loss coefficients, which contains those extrapolated ones, and the relative inlet angle tangent values can be fitted, then from the derived function of this fitting function and the extrapolated flow field data, the derivation of extrapolated loss coefficients to relative inlet angle tangent values will be find out.

The fitting methods based on the extrapolated flow field can provide more aerodynamic data at the unstable operating points to the stall inception model. Figure 7 shows the variation of some aerodynamic data at the inlet of the four blade

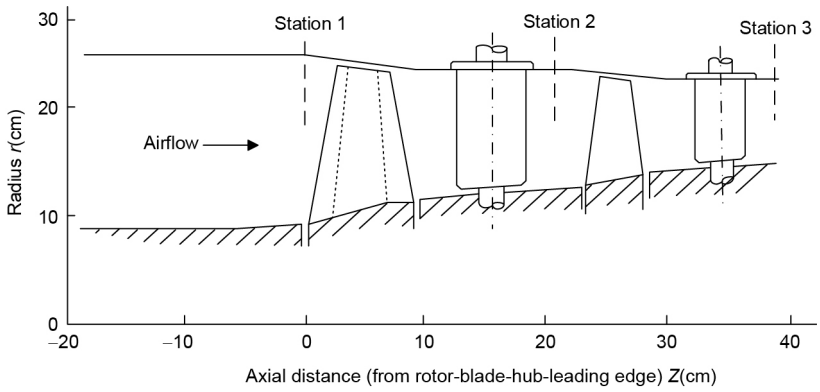

Figure 5 Flow path of NASA two stage fan.

Table 1 Design parameters of NASA two stage fan

Design parameters	Blades number	Aspect ratio	Design speed (r/min)	Stage total pressure ratio	Stage adiabatic efficiency
Rotor one	43	1.56	16042.80	1.59	0.848
Stator one	34	1.98	0		
Rotor two	38	1.89	16042.80	1.509	0.870
Stator two	42	1.85	0		

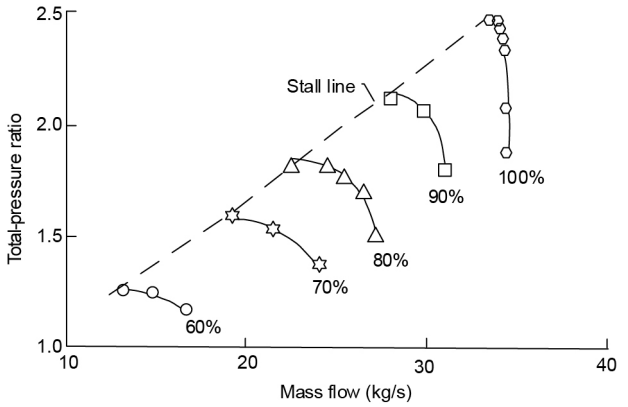

Figure 6 Overall performance of NASA two-stage fan.

Table 2 Relative inlet Mach numbers of the NASA two stage fan at the blade tip

Operating speed	First rotor	First stator	Second rotor	Second stator
100%	1.37	0.62	1.21	0.57
80%	1.05	0.49	0.98	0.45

rows with the mass flow, such as axial velocity V_z, static pressure P_s, loss and its derivation. At the zone with smaller mass flow, the V_z reduces, the P_s increases gently and the loss decreases initially and then increases.

The theoretical prediction of the stall inception point is shown in Figure 8. The x-axis represents the mass flow and the y-axis indicates the damping factor (DF) of the precursor wave, which is defined as $r_m\omega_I/(mU_0)$. When the damping factor DF goes to zero, the stability of the compressor system is changed from stable state to unstable state and the stall inception point can be obtained. There are two arrows in Figure 6, which indicate the stall points of the theoretical prediction and experimental observation respectively. It can be seen that the error between the theoretical prediction and experimental observation is about 5%. While as mentioned before, only first five data points are obtained from experiment, and the DF curve in small mass flow zone comes from extrapolation, so as to the stall point of this theoretical prediction. For this reason, the theoretical prediction of the stall inception point is relatively optimistic.

As for the propagation speed of the precursor wave for this case, the relative speed (RS), which is defined as $60\omega_r/(2\pi m\Omega)$, is about 60.1% near the stall point.

3.3 Model validation on NASA two-stage fan at 100% design operating speed

Figure 9 shows the variation of the related aerodynamic data with the mass flow at 100% design operating speed. The trends of these variations are similar with the results at 80% design operating speed.

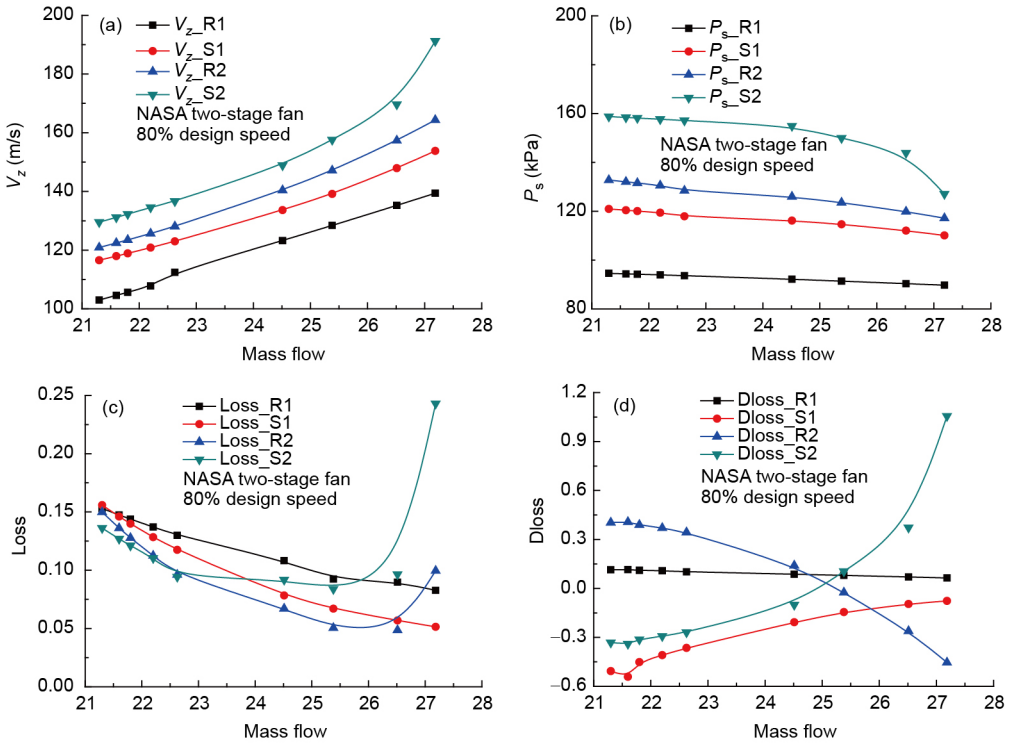

Figure 7 (Color online) Aerodynamic parameters of NASA two-stage fan at 80% design speed. (a) Axial velocity; (b) static pressure; (c) loss coefficient; (d) derivation of loss coefficients.

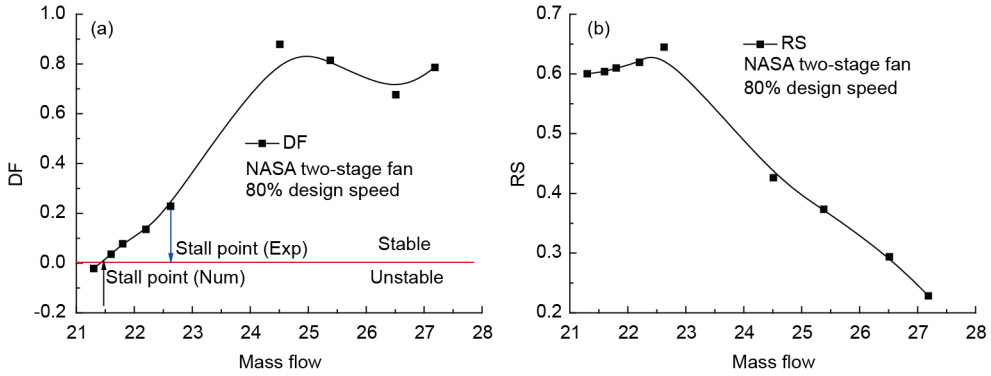

Figure 8 (Color online) Stability prediction of NASA two-stage fan at 80% design speed. (a) Damping factor DF; (b) relative speed RS.

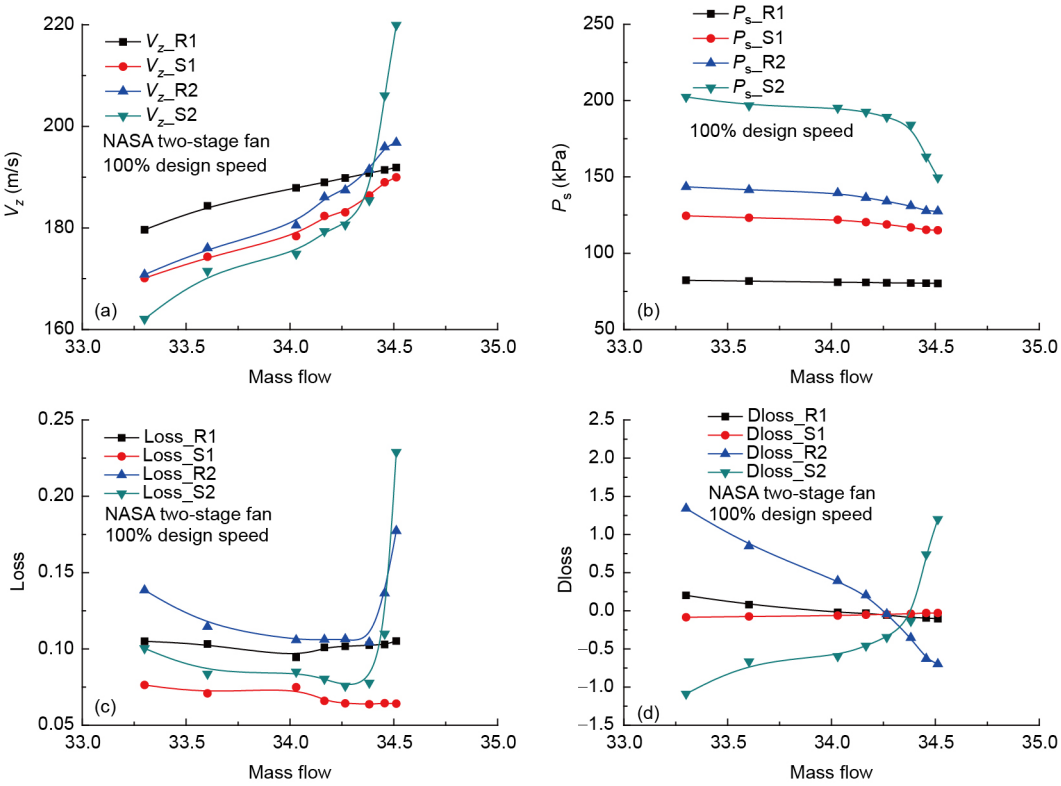

Figure 9 (Color online) Aerodynamic parameters of NASA two-stage fan at 100% design speed. (a) Axial velocity; (b) static pressure; (c) loss coefficient; (d) derivation of loss coefficients.

Figure 10 shows the prediction results of the NASA two-stage fan at 100% design operating speed. It is noted that with the throttle control the flow rate decreases, and the DF decreases too near the stall point. When the flow rate is 33.9 kg/s, the DF passes through the critical value of stability, and the relative rotating speed of this model numerical result is 52.5% design operating speed. The relative error of the stall inception point is 0.9% comparing with the experiment result, which is a reasonable prediction of accuracy. In this case, the first seven data points are all obtained from experiment, and the theoretical prediction of stall point is from the fitting curve not the extrapolated curve, so the theoretical prediction of the stall inception point here is relatively pessimistic.

4 Further analysis and discussion

4.1 The effects of time delay on compressor stability

In order to obtain the unsteady effects of compressor flow, it is necessary to test the effect of time delay on the predicting results. Normally, the accurate value of time delay should be obtained from the experiment measurement. In ref. [30], some methods were introduced to reflect the dynamic response characteristic of compressor. While in this paper, the first order delay relationship has been chosen to indicate the effects of time delay on compressor stability, and it can be described as $\tau_{\text{loss}} = c / W_c$, where c is the chord length of blade, and W_c is the mean velocity of flow in cascade.

The present investigation is aimed at the different situations of no time delay, a given time delay and double time delay. Figure 11 shows the calculation results of perturbation wave decay factor and relative circumferential velocity with different time delay for NASA two-stage compressor under 100% design working speed. From this figure, there are only a little effects of time delay on whole compressor stages, which can be neglected, and the effects on circumferential velocity are also not much.

4.2 The effects of blade span-chord ratio on compressor stability

The blade span-chord ratio is also an important factor in affecting compressor stability. Compared to ref. [30], NASA report [28] hoped to realize the stability enhancement by decreasing the span-chord ratio of first stage. In order to discover the effects of blade span-chord ratio on compressor stability margin, this paper has tried to use theoretical model to investigate these effects by purely changing the blade chord length in model. And for the briefness of this research, all aerodynamic parameters are from experimental data, the blade chord length is the only variable parameter. Figure 12 shows the calculation results of perturbation wave decay factor and relative circumferential velocity with 80%, 100% and 120% chord length for NASA two-stage compressor under 100% design working speed. In this figure, when the loss and relative inlet angle are same with the experiment data, a lower span-chord ratio can enhance the stability of whole compressor, which is similar to the consideration in ref. [28].

4.3 The effects of loss coefficient on compressor stability

Nenni and Ludwing [14] gave the analytical expression of loss coefficient and stability in his 2-D stability model, and his research results demonstrated that loss coefficient is a significant factor which can affect the compressor stability. From Figure 7, the results show that with the throttle progress the loss coefficient of second stage changes more obviously than the first stage, and the derivative value with respect to inlet angle also changes more in second stage. Combined with the prediction results of blade span-chord ratio, the present investigation indicates that because of the low span-chord ratio in first stage and high span-chord ratio in second stage, this two-stage compressor shows less stability in second stage. It is believed that such match design may lead to restricting the stability range of whole two-stage compressor.

4.4 The effects of different fitting orders on compressor stability

During the process of extrapolating flow field parameters from experiment data, this paper has tried to use different fitting orders to observe its effects on stall prediction. Figure 13

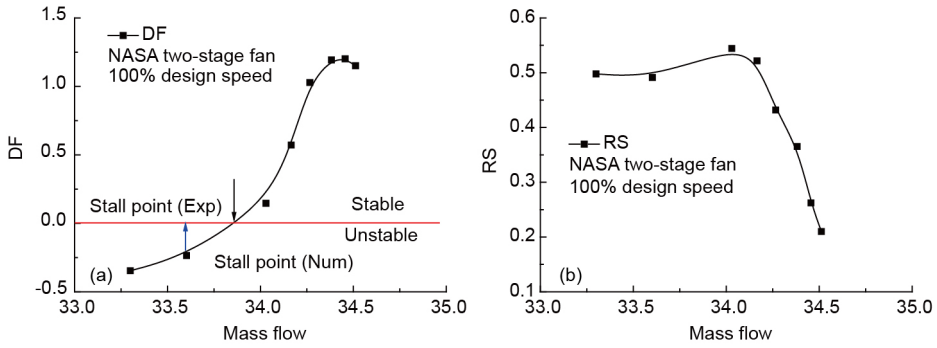

Figure 10 (Color online) Stability prediction of NASA two-stage fan at 100% design speed. (a) Damping factor DF; (b) relative speed RS.

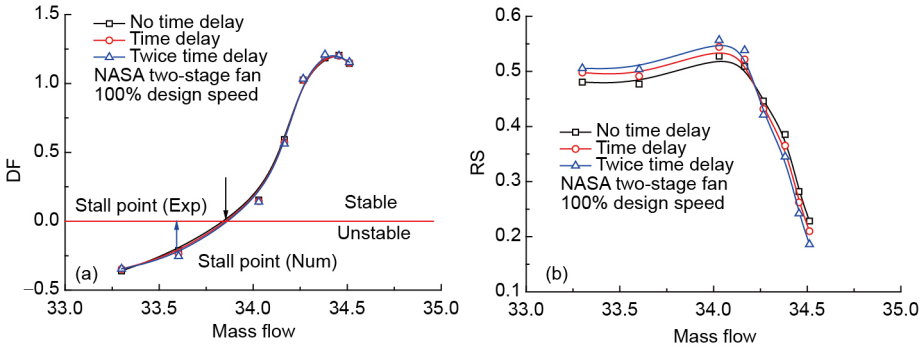

Figure 11 (Color online) The effects of time delay on NASA two-stage compressor stability under 100% design working speed. (a) Damping factor DF; (b) relative speed RS.

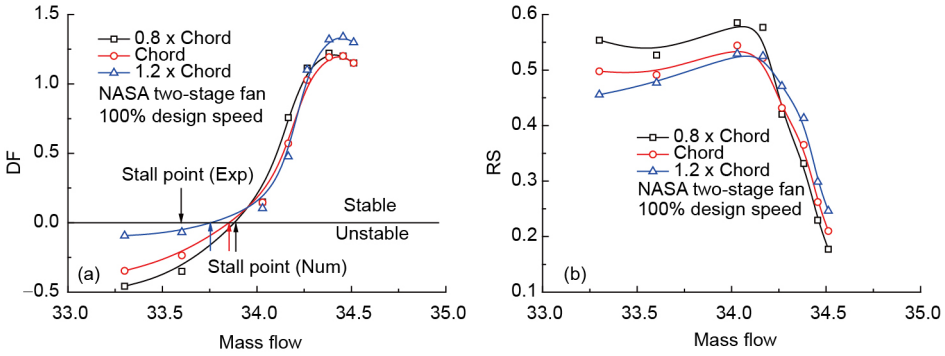

Figure 12 (Color online) The effects of blade span-chord ratio on the stability of NASA two-stage compressor under 100% design working speed. (a) Damping factor DF; (b) relative speed RS.

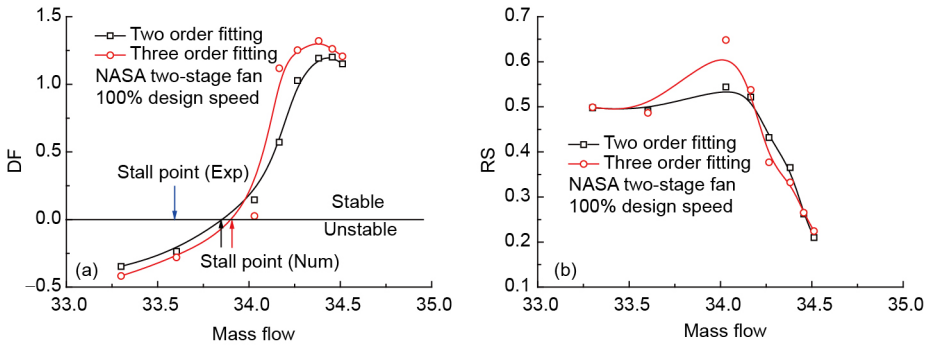

Figure 13 (Color online) The effects of different fitting orders on NASA two-stage compressor under 100% design working speed. (a) Damping factor DF; (b) relative speed RS.

reveals the theoretical predictions of extrapolation calculation by using quadratic fit and cubic fit. In this figure, it is obvious that there is a little difference at the prediction of stall point by using different fitting orders but the variation trends of compressor stability are similar.

5 Conclusion

1) A stall inception model for multi-stage compressors is developed in this paper, and the NASA two-stage fan is used to validate the effectiveness of this model.

2) The computation results of compressor stall inception points are in close agreement with experimental data at 100% and 80% design speeds, respectively.

3) The present work has also investigated how to obtain the compressor aerodynamic parameters at the unstable working point based on the extrapolation method and this model is capable of predicting mass flow at the stall-onset point of multi-stage compressor with a reasonable accuracy.

4) This paper does some further discussions about the effects of delay time, span-chord ratio, loss coefficient and fitting order on stall inception prediction, these results thus indicate the accuracy and reliability of the present theoretical model on the calculation investigation about multi-stage compressor stability.

This work was supported by the National Natural Science Foundation of China (Grant Nos. 51576008 & 51236001), the National Basic Research Program of China (Grant No. 2012CB720201), Aeronautical Science Foundation of China (Grant No. 2014ZB51018), the Collaborative Innovation Center for Advanced Aero-Engine of China, and the Fundamental Research Funds for the Central Universities.

1 Hendricks G J, Sabnis J S, Feulner M R. Analysis of instability inception in high-speed multi-stage axial-flow compressors. In: Proceedings of ASME 1996 International Gas Turbine and Aeroengine Congress and Exhibition. Birmingham, UK, 1996
2 Longley J P. Calculating the flow field behaviour of high-speed multistage compressors. In: Proceedings of ASME 1997 International Gas Turbine and Aeroengine Congress and Exhibition. Orlando, 1997
3 He L. Computational study of rotating-stall inception in axial compressors. J Propul Power, 1997, 13: 31–38
4 Gong Y, Tan C S, Gordon K A. A computational model for short wavelength stall inception and development in multistage compressors. In: Proceedings of ASME 1998 International Gas Turbine and Aeroengine Congress and Exhibition. Stockholm, 1998
5 Sun X, Liu X, Hou R, et al. A general theory of flow-instability inception in turbomachinery. AIAA J, 2013, 51: 1675–1687
6 Liu X, Sun D, Sun X. Basic studies of flow-instability inception in axial compressors using eigenvalue method. J Fluids Eng, 2014, 136: 031102
7 Liu X, Zhou Y, Sun X, et al. Calculation of flow instability inception in high speed axial compressors based on an eigenvalue theory. J Turbomach, 2015, 137: 061007
8 Sun X F, Ma Y F, Liu X H, et al. Flow stability model of centrifugal compressor based on eigenvalue approach. AIAA J, 2016, 54: 2361

9 Chen J P, Hathaway M D, Herrick G P. Prestall behavior of a transonic axial compressor stage via time-accurate numerical simulation. J Turbomach, 2008, 130: 041014
10 Sears W R. Rotating stall in axial compressors. J Appl Math Phys (ZAMP), 1955, 6: 429–455
11 Emmons H W, Pearson C E, Grant H P. Compressor surge and stall propagation. ASME Trans, 1955, 77: 455–469
12 Day I J. Stall, surge and 75 years of research. J Turbomach, 2016, 138: 011001
13 Stenning A H. Rotating stall and surge. J Fluids Eng, 1980, 102: 14–20
14 Nenni J P, Ludwig G R. A theory to predict the inception of rotating stall in axial flow compressors. In: Proceedings of the 7th Fluid and Plasma Dynamics Conference. Palo Alto, CA, 1974
15 Ludwig G R, Nenni J P. Basic studies of rotating stall in axial flow compressors. Technology Report. Calspan Advanced Technology Center Buffalo NY Aerodynamic Research Dept, 1979
16 Bonnaure L P. Modeling high speed multistage compressor stability. Doctoral Dissertation. Massachusetts: Massachusetts Institute of Technology, 1991
17 Takata H, Nagashima T. Rotating stall in three-dimensional blade rows subjected to spanwise shear flow. In: Proceedings of the 7th International Symposium on Air Breathing Engines. Beijing, China, 1985
18 Gordon K. Three-dimensional rotating stall inception and effects of rotating tip clearance asymmetry in axial compressors. Dissertation of Doctoral Degree. Massachusetts: Massachusetts Institute of Technology, 1998
19 Gorrell S E, Russler P M. Stall inception in a high-speed low aspect ratio fan including the effects of casing treatments. In: Proceedings of ASME 1994 International Gas Turbine and Aeroengine Congress and Exposition. The Hague, 1994
20 Sun X F. On the relation between the inception of rotating stall and casing treatment. In: Proceedings of 32nd Joint Propulsion Conference and Exhibit. Lake Buena Vista, FL, 1996
21 Sun X, Sun D, Yu W. A model to predict stall inception of transonic axial flow fan/compressors. Chin J Aeronautics, 2011, 24: 687–700
22 Sun D, Liu X, Sun X. An evaluation approach for the stall margin enhancement with stall precursor-suppressed casing treatment. J Fluids Eng, 2015, 137: 081102
23 Sun X, Sun D, Liu X, et al. Theory of compressor stability enhancement using novel casing treatment, Part I: Methodology. J Propul Power, 2014, 30: 1224–1235
24 Sun D, Liu X, Jin D, et al. Theory of compressor stability enhancement using novel casing treatment, Part II: Experiment. J Propul Power, 2014, 30: 1236–1247
25 Sun D K, Nie C Q, Liu X H, et al. Further investigation on transonic compressor stall margin enhancement with stall precursor-suppressed casing treatment. J Turbomach, 2016, 138: 021001
26 Liu X, Sun D, Sun X, et al. Flow stability model for fan/compressors with annular duct and novel casing treatment. Chin J Aeronautics, 2012, 25: 143–154
27 Dong X, Liu X, Sun D, et al. Experimental investigation on SPS casing treatment with bias flow. Chin J Aeronautics, 2014, 27: 1352–1362
28 Urasek D C, Gorrell W T, Cunnan W S. Performance of two-stage fan having low-aspect-ratio first-stage rotor blading. Technology Repot. NASA, 1979
29 Howard III, Joseph S. Improved methods for modeling dynamic stage characteristics. Dissertation of Masteral Degree. Virginia: Virginia Polytechnic Institute and State University, 1999
30 Cunnan W S, Stevans W, Urasek D C. Design and performance of a 427-meter-per-second-tip-speed two-stage fan having a 2.40 pressure ratio. Technology Repot. NASA, 1978